Full reciprocal-space mapping up to 2000 K under controlled atmosphere: the multipurpose QMAX furnace

René Guinebretière, Stephan Arnaud, Nils Blanc, Nathalie Boudet, Elsa Thune, David Babonneau, Olivier Castelnau

manuscript nb5267 for review

JOURNAL OF APPLIED CRYSTALLOGRAPHY

Full reciprocal space mapping up to 2000 K under controlled atmosphere: the multi-purpose QMAX furnace

Rene Guinebretiere, Stephan Arnaud, Nils Blanc, Nathalie Boudet, Elsa Thune, David Babonneau and Olivier Castelnau

Category: *research papers*

Co-editor:

Dr A. Borbely

Directeur de Recherche, Ecole National Supérieure des Mines, Saint-Etienne, France

Telephone: +33 (0)4 77 42 02 79

Fax: +33 (0)4 77 42 00 00

Email: andras.borbely@mines-stetienne.fr

Submitting author:

René Guinebretière

IRCER, 12 rue Atlantis, Limoges, 87068, France

Telephone: 0631803737

Fax: ?

Email: rene.guinebretiere@unilim.fr

Full reciprocal space mapping up to 2000 K under controlled atmosphere: the multi-purpose QMAX furnace

René Guinebretière[a*], Stephan Arnaud[b], Nils Blanc[b], Nathalie Boudet[b], Elsa Thune[a], David Babonneau[c], Olivier Castelnau[d]

[a]Université de Limoges, IRCER, UMR 7315, CNRS, Centre Européen de la Céramique, F-87068 Limoges, France

[b]Université Grenoble Alpes, CNRS, Institut Néel UPR CNRS 2940, 38000 Grenoble, France.

[c]Université de Poitiers, Institut Pprime, Département Physique et Mécanique des Matériaux, UPR CNRS 3346, SP2MI, TSA 41123, 86073 Poitiers Cedex 9, France

[d]Laboratoire PIMM, UMR CNRS 8006, ENSAM, CNAM, 151 Bd de l'Hôpital, 75013 Paris, France

*Authors to whom correspondence should be addressed: rene.guinebretiere@unilim.fr

Synopsis This article presents the capability of the QMAX furnace devoted to reciprocal space mapping through X-ray scattering at high temperature up to 2000 K.

Abstract A furnace that covers the temperature range from room temperature up to 2000 K has been designed, built-up and implemented on the D2AM beamline at the ESRF. This QMAX furnace is devoted to the full exploration of the reciprocal hemi-space located above the sample surface. It is well suited for symmetric or asymmetric 3D reciprocal space mapping. Thanks to the hemispherical design of the furnace, 3D grazing incidence small or wide angle scattering or diffraction measurements are possible. Inert or reactive experiments are performed at the atmospheric pressure under controlled gas flux. We demonstrate that the QMAX furnace allows monitoring of structural phase transitions as well as microstructural evolutions at the nanoscale such as self-organization processes, crystal growth or strain relaxation. A time-resolved oxidation *in situ* experiment illustrates the capability to probe the high temperature reactivity of materials.

Keywords: Reciprocal space mapping, high temperature, *in situ*, Structural and microstructural evolutions under extreme conditions, controlled atmosphere

1. Introduction

One of the current issues in material science is to be able to determine *in situ* the structural and microstructural evolutions of materials as a function of external constraints (Tao & Salmeron, 2011; Villanova et al., 2017). X-ray scattering (diffuse scattering, small angle X-ray scattering, diffraction) or absorption (tomography, absorption spectroscopy) experiments are non-destructive and very well suited for the characterization of actual materials during their elaboration or in operating conditions. Nevertheless, dynamical experimental studies able to evidence in convenient time-scale the *in situ* evolution of materials under very high temperature or pressure, mechanical constrains or environmental atmosphere variations through gas flows, require the use of high flux X-ray sources. It is well-known that the 3rd generation of synchrotron radiation sources are very useful facilities in this field (Montano & Oyanagi, 1999). Nowadays, the association of such X-ray sources and 2D-position sensitive detectors allows the collection of scattering or diffraction patterns in a second or even shorter time scale (Basolo *et al.*, 2007; Bergamaschi *et al.*, 2010; Ors *et al.*, 2019) and full 3D exploration of the reciprocal space can be done around any reciprocal lattice node (RLN) within one hour (Cornelius *et al.*, 2012) or less (Leake *et al.* 2019). For many years, the structural or microstructural evolutions (*i.e.* phase transitions, thermal expansion, grain growth, defect mobility etc.) as a function of temperature or pressure are studied through *in situ* X-ray scattering based methods. Nevertheless, in many cases, the samples have to be prepared in such a way that they fit the experimental constrains related to the use of high-temperature furnaces or diamond anvil cells. Consequently, the characterized samples are often very different, especially from the microstructural point of view, from the actual materials under consideration. It is thus an on-going work to develop X-ray scattering set-ups well suited to capture the structural evolutions of single crystal surfaces, thin films, nanostructures as well as 3D bulk polycrystalline materials under reactive or non-reactive atmosphere at temperature higher than 1250 K with a convenient time scale resolution.

Chemists who synthesize new compounds or develop crystal chemistry studies commonly realize high temperature X-ray diffraction (XRD) experiments. In most cases, such studies are done on powdered samples often put into capillary sample holders. The use of such capillary sample holders under the Debye-Scherrer diffraction geometry (Guinebretière, 2007) associated with one-dimensional position sensitive gaseous (Benard *et al.*, 1996; Muller *et al.*, 1997) or solid state (Pickup *et al.*, 2000; Sarin *et al.*, 2009) curved detectors allows high angular resolution diffraction patterns to be collected in a short time at temperatures as high as 1250 K. Nevertheless, such an approach is far from the characterization of single crystal surfaces, thin films or bulk materials. On the other hand, cylindrical furnaces where a platinum foil strips act simultaneously as heating element and sample holder have been developed for many years (Koppelhuber-Bitschnau *et al*. 1996). However, a quite large expansion of this metallic strips and subsequent sample displacement are induced by the temperature increase. Although such setup has been largely used, accurate sample positioning as a function of

temperature is still a difficult task (Brown *et al.*, 1993; Misture *et al.*, 2002; Beck & Mittemeijer, 2002) and it is well known that sample displacement with respect to the goniometer axes has a great influence on the accuracy of the d-spacing measurements (Masson *et al.*, 1996). This drawback can be solved using cylindrical furnaces in which the samples are put on top of an alumina disk located on the spinning stage that corresponds to the azimuthal rotation around the sample surface (Gualtieri *et al.*, 1999; Estermann *et al.*, 1999; Guinebretière *et al.*, 2007). Heating of the samples is usually realized using conventional high temperature heaters located around the sample holder. Association of this set-up with a translational stage along the azimuthal φ-rotation axis, allows one to continuously compensate the sample holder thermal expansion (Gualtieri *et al.*, 1999; Guinebretière *et al.*, 2007). One of the most significant achievement using this configuration is certainly the furnace built by M. Yashima *et al.* on the 4B2 beamline at the Photon Factory in Japan (Yashima *et al.*, 2006). They demonstrated that the combination of such a cylindrical furnace and a multiple detector allows high-angular resolution XRD patterns to be recorded at temperatures as high as 1900 K on a number of ceramic materials and the corresponding structures to be described (Yashima, 2002; Yashima & Tanaka 2004).

The devices that we briefly described above are build-up in such a way that whatever the detectors are, the X-rays scattered by the sample can be recorded only if they are scattered in the so-called "diffraction plane", *i.e.* the plane containing both the direction of the primary X-ray beam and the normal to the sample surface. Taking into account the limited width of the window of the cylindrical furnaces, very few X-ray beams scattered out of this plane can reach the detector. This is the main drawback of such set-ups, which induces two different consequences: firstly it strongly limits the interest of the use of any 2D-detector that are nowadays more and more used especially for 2D or 3D exploration of the reciprocal space; Secondly it forbids in-plane measurements such as Grazing Incidence Small angle X-ray Scattering (GISAXS) or Grazing Incidence Diffraction (GID).

During the last years, we developed a new furnace allowing reciprocal space maps (RSM) to be recorded up to 2000 K either close to the centre of the reciprocal space, *i.e.* in the small angle scattering regime, or around any diffraction nodes. We report here on the use of this set-up, called the "QMAX furnace" that we have implemented on the French Collaborating Research Group (F-CRG) D2AM beamline at the ESRF (Chahine *et al.*, 2019). The QMAX furnace works in reflection mode and it allows GISAXS and GID to be collected as well as conventional out-of-plane diffraction patterns under symmetric or asymmetric configurations. Beside the very high temperatures that are under consideration, one of the main characteristics of the QMAX furnace is that the experiments are realized under controlled gas flux. *In situ* reactive experiments can thus easily be performed.

2. Description of the QMAX furnace

A global view of the QMAX furnace is reported in fig. 1a and a cross-sectional drawing is reported fig. 1b. The implementation on the D2AM beamline goniometer is illustrated in fig. 1c. In order to be able to characterize bulk polycrystalline samples as well as thin films or single crystal surfaces, the furnace has been designed for experiments in the reflection geometry under asymmetric incidence angles on flat samples (Guinebretière, 2007). The confinement of the atmosphere around the sample is realized using a hemispherical beryllium dome and the furnace is designed in such a way that the detector can collect all the X-rays scattered in the half-space above the sample. One can notice that this geometry is similar to that chosen by the Anton-Paar company for its "DHS" heating stage series (Kotnik *et al.*, 2006). Nevertheless, the maximal temperature accessible using these furnaces is, under optimal conditions, 1350 K that is far below to the accessible temperature with the QMAX furnace. Moreover, no accurate control of the gas flux is implemented on the DHS devices.

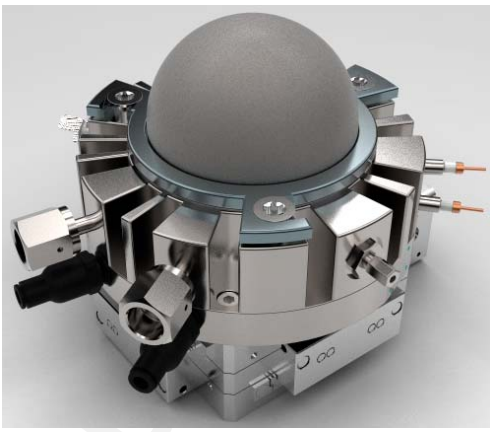

(a) picture of the furnace

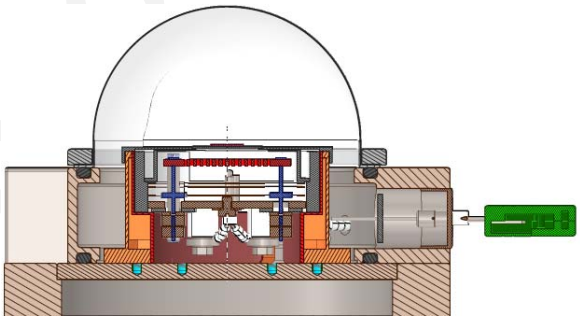

(b) cross-sectional drawing of the furnace

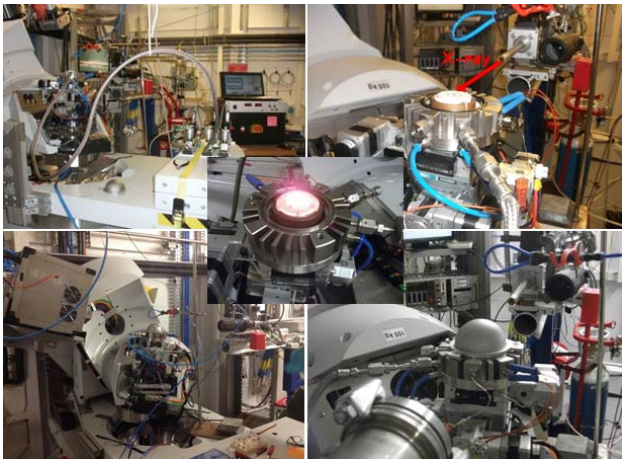

(c) pictures showing the furnace at high temperature on the goniometer and all the associated devices.

Figure 1. The QMAX furnace in its working environment at the D2AM beamline.

The heating of the samples is ensured by a 80Pt-20Rh plate put onto an alumina flat holder specifically designed so that it retains its integrity despite the differential expansion associated with temperature gradients. The samples themselves are fixed onto the heating element in a way depending on their nature (see below). Very near to the sample heating stage, a flowing water cooling device made of two coaxial copper cylinders allows the steel body of the furnace to be maintained at the room temperature (RT). Additionally, an airflow shower located above the beryllium dome, *i.e.* above the entire furnace, allows keeping the temperature of the dome below 350 K to prevent the beryllium from oxidation whatever

the temperature of the sample is.

The QMAX furnace internal temperature is measured using a Pt – 10%Rh-Pt thermocouple located at roughly one millimeter underneath the sample. The temperature evolution is driven by a Nanodac controller from Eurotherm by Schneider Electric company. It is linked to the computer driving all the experimental set-up and thus the temperature is recorded in a global data file. The PID furnace parameters can be fully controlled by the computer and adjusted as a function of the temperature. The heating rate can be as high as 50 °C/min. The furnace itself is mounted above a goniometric motorized head made of two crossed cradles and two translations put on top of the kappa stage of the D2AM goniometer (Chahine *et al.*, 2019). All along this article, the description of the experiments will be done using the classical convention with respect to the goniometer rotation axis and reciprocal space vector components (Guinebretière, 2007). The ω-axis gives the incidence angle of the primary beam onto the sample surface, the φ-axis is orthogonal to the ω–axis and normal to a reference plane chosen by the experimentalists (the sample surface, any diffracting plane of a single crystal, etc.), and the χ-axis is orthogonal to the two others. After convenient positioning process of the sample with respect to these goniometer axes using the motorized goniometric head, the $\overrightarrow{q_x}$, $\overrightarrow{q_y}$ and $\overrightarrow{q_z}$ components of the scattering vectors are respectively collinear to the χ-axis, ω–axis and φ-axis unit vectors.

Using such a set-up, flat samples located into the furnace can be carefully aligned before the X-ray scattering measurements at any temperature with respect to their surface or any of their diffracting planes with an angular accuracy of a few thousandths of degree (Boulle *et al.*, 2001). Translational displacement of the samples due to the thermal expansion can be fully compensated using a z-translation situated below the goniometric head. After a first determination of the thermal expansion of the sample, an automatic compensation of this expansion can be implemented in the code driving the goniometer. Thus, whatever the temperature is, the surface of the sample contains the cross point of the ω, φ and χ rotation axes of the diffractometer. This allows solving the well-known sample displacement problem underlined by numerous authors (see above). As already said, the QMAX furnace is designed for the realization of experiments at atmospheric pressure under inert or reactive gas flow. Chemical reactions can be followed under a given gas or a mixture of two different gases of any kind introduced into the furnace through computer-driven flowmeters allowing a gas flux up to one litre per minute with a few millilitres per minute accuracy. Finally, the main technical characteristics of the QMAX furnace are given Table 1.

Table 1 .Main characteristics of the QMAX furnace

Geometry of the x-ray scattering measurements	Reflection mode under grazing or any incidence angle in small angle range or around any RLN located above the sample surface	
Heating conditions	Heating element	80 at% platinum – 20 at% rhodium alloy plate
	Maximal temperature	2000 K
	Maximal heating / cooling rate	50 K/min
	Working pressure	Atmospheric pressure
	Gas flux	Mixing of any two different gas with respect to the conventional security rules
		Few millilitre per minute to one litre per minute
Bulk single crystalline or polycrystalline samples	Typical size of the surface	10 x 10 mm
	Typical sample thickness	Few tenths of millimetre to few millimetres
Powdered samples	The powder is located in counterbore (0.5 mm depth and 12.5 mm of diameter) machined on a sapphire cylindrical piece	
Global dimension of the furnace	Stage diameter	140 mm
	Stage height	96.5 mm with the dome
Confinement around the sample	Beryllium dome	

One of the main characteristics of a furnace is of course the maximal temperature that can be reached during the experiment. It is important to note that the temperature of interest is that one of the sample and not the value of the temperature set-point. We made a large number of experiments and we observed that the maximal accessible temperature is depending on the nature of the samples and more specifically on their thermal properties that themselves are related to the composition of the samples but also to their state (*i.e.* if it is a single crystal, a powder or a bulk sample). We report on fig. 2 parts of diffraction patterns recorded on the D2AM beamline on a powdered sample made of a mixing of industrial zirconia powder and the NIST SRM 676a alumina powder. The energy of the x-ray beam was fixed at 17,9 keV. Before each diffraction measurement at any temperature the sample position along the *z*-axis is corrected as explained above. According to Touloukian *et al.* (Touloukian *et al.*, 1977), the temperature of the sample can be determine based on the thermal expansion coefficients along the $\vec{a}$ and

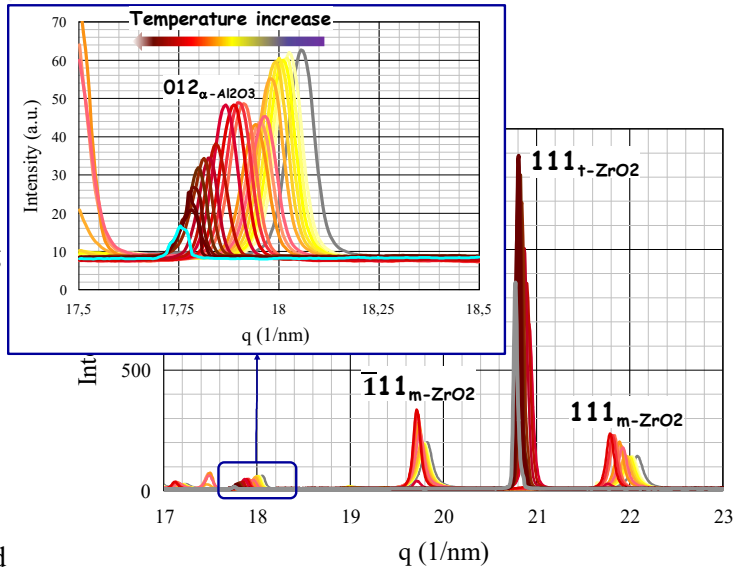

Figure 2. Thermal expansion of α-alumina in a zirconia-alumina powder mixing. The lower *Q*-position of the 012 diffraction peak is corresponding to a temperature of 2100 K.

$\vec{c}$ axis of alumina. The main diffraction peaks observed in the patterns are that of both monoclinic and tetragonal zirconia. Zooming with respect to the q-axis between 17.5 and 18.5 nm^{-1} allows evidencing the displacement of the 012 diffraction peak of alumina with respect to the increase of the temperature. Of course increasing of the temperature induces a decrease of the q-value of the peak position. At higher temperature, this position is roughly equal to 17.755 nm^{-1}. According to Touloukian *et al.* (Touloukian *et al.*, 1977), this is corresponding to 2090 K and this is the higher sample temperature that we reached. We nevertheless fix the maximal working temperature of the QMAX furnace to 2000 K (see table 1).

In the following sections, we will present different cases of *in situ* high temperature studies realized on the D2AM beamline at the ESRF using the QMAX furnace described above. Both the scientific topics that are concerned and the type of samples studied were very different. The first case addresses the self-organization processes on single crystal vicinal surfaces. The second study illustrates the capability of the set-up to follow the thermal expansion and to evidence phase transitions and crystal growth in a crystalline powder as a function of the temperature or during isothermal treatments. The third case concerns a similar approach on bulk polycrystalline samples. It evidences the relationship between phase transition and residual stress relaxation processes. In the last example, we illustrate the capability of our set-up to follow the oxidation process of metallic plates during rapid increase of the temperature (20 K/min). In all the cases, the experimental results that we present are not discussed on the point of view of their meaning with respect to material science. Such discussions are out of the scope of this article and they will be presented in forthcoming papers.

3. 3D-Grazing Incidence Small Angle X-ray Scattering at high temperature on vicinal single crystal surfaces

Thermal treatment of vicinal surfaces of single crystals usually induces step bunching that results in the formation, through a self-organization process, of periodic hill-and-valley structures at the mesoscopic scale (Misbah *et al.*, 2010). These ordered surfaces can be very well imaged through near-field microscopy observations. Nevertheless, such local observations probe micrometric areas and more global characterization methods such as GISAXS are also mandatory.

Sapphire, *i.e.* α-alumina single crystals, is commonly used as substrate for the growth of various oxide nanostructures used in Light-Emitting Diodes (Nakamura, 1998; Koester *et al.*, 2011), zinc oxide nanodots or nanowires for electroluminescent devices (Huang *et al.*, 2001; Eaton *et al.*, 2016) as well as lithium niobate epitaxial thin films for electro-optical modulators (Boulle *et al.*, 2009). It has been shown that the use of sapphire vicinal substrates allows controlling the growth process and the size or the shape of the dots grown onto such surfaces (Lee, 2007; Ago *et al.*, 2007; Bachelet *et al.*, 2007a; Bachelet *et al.*, 2007b; Camelio *et al.*, 2007). The crystallographic structure of sapphire is

described in the trigonal $R\bar{3}c$ space group and it is usually represented in the hexagonal multiple cell. Throughout this paper, indexations will be given with respect to this hexagonal setting.

A few years ago, we demonstrated that thermal treatment of sapphire vicinal surfaces obtained by cutting the single crystals with a miscut angle of 10° with respect to the (006) planes allows promoting the formation of well-ordered surfaces exhibiting periodic steps with a width of a few tens of nanometers, depending on the temperature, the duration and the atmosphere of the thermal treatment (Thune *et al.*, 2017; Matringe *et al.*, 2017). However, significant ordering effect is observed only when the thermal treatment is realized at temperatures higher than 1250 K in air or oxygen-rich atmosphere. In addition, it is worth noting that one of the most remarkable results achieved in these studies is the observation of 1D as well as 2D ordered surfaces (Matringe, 2016). The previous investigations left open the question whether the 2D structure appears by a rearrangement of the 1D one or these two structures are an alternative each for the other. Answering this question requires to be sure that the observed area of the sample is always the same for each thermal treatment condition; it is thus very difficult to give an accurate input relative to this question through *ex situ* measurements, which would imply that a set of samples initially strictly identical is used. We have thus make use of the new QMAX furnace to follow the self-ordering process through *in situ* GISAXS measurements performed under isothermal conditions. However, observation of significant evolution for a reasonable amount of time (*i.e.* few hours) compatible with the availability of the synchrotron beamtime requires the achievement of measurements at least at 1450 K under pure oxygen continuous flux. While each GISAXS map corresponds roughly to a (q_y,q_z) 2D slice of the reciprocal space, 3D measurements are obtained by recording a large set of (q_y,q_z) maps at different azimuthal angles (around the φ-axis). It is well known that the intensity distribution collected through GISAXS 2D measurements is very sensitive to the z-position of the sample and to the angle of incidence of the primary X-ray beam onto the studied surface. It is therefore very important that these two parameters are kept constant all along the 3D measurement with an accuracy of 10 microns and 0.01 degree respectively.

We followed continuously the self-organization process of a sapphire vicinal surface during isothermal treatment at 1600 K under pure oxygen flux during 40 hours. The GISAXS signal was recorded at 8 keV with an incidence angle of 0.30° and using the 3.2 version of the XPAD 2D pixel hybrid detector (Medjoubi *et al.* 2010; Le Bourlot *et al.* 2012) located at 5050 mm from the sample. The surface was elaborated with a miscut angle equal to 10° with respect to the (006) sapphire planes and in such a way that the step edges were parallel to the $[1\bar{1}0]$ direction. The azimuthal orientation was determined from the diffraction of the (1 1 12) planes and the zero value of the φ rotation was defined as the position where these planes were under diffraction condition, *i.e.* with the primary beam orthogonal to the [110] direction. Because the $[1\bar{1}0]$ direction of sapphire is orthogonal to the [110] one, in this situation the step edges are strictly parallel to the primary X-ray beam. After

convenient alignment, we were able to record 3D-RSMs made of 721 (q_y,q_z) 2D-maps collected with a 0.5° rotation step around the φ-axis. A full 3D-RSM was obtained with a good signal-to-noise ratio in only 15 minutes. Because significant evolution of the surface took several hours, we can consider that time-resolved measurements were thus carried out.

During the temperature increase, because of the thermal expansion not only of the sample but also of some parts of the heating sample holder, the sample surface shifts and can be more or less disoriented. As mentioned above, the entire furnace is located on top of the goniometric head, therefore the correct height as well as the orientation of the sample can be recovered at any temperature. After reaching the target temperature, the sample surface was thus fully realigned. Furthermore, the true temperature of the sample was determined according to the thermal expansion law of the *c* cell parameter of sapphire (Touloukian *et al.*, 1977) through the measurement of the position of the 0,0,6 sapphire RLN. It is noticeable that neither any shift nor twist of the sample was observed all along the roughly two-days isothermal treatment at 1600 K.

Projections along the q_z axis of some of the obtained 3D-RSMs are reported in fig. 3. Before any thermal treatment, the vicinal surface is made of steps without any order and the scattering signal reported in fig. 3a is isotropic. After 1 hour and 45 minutes, the projection of the 3D-RSM exhibits very clearly a scattering line along the q_y direction which, according to the sample orientation, is due to the ordering of the steps. All along the thermal treatment, this scattering line is observed. Additional structures in the scattered signal progressively appear onto the maps recorded after more than 5 hours, with specific diffuse scattering lines being observed. According to *ex situ* GISAXS measurements (Matringe, 2016; Matringe *et al.* 2020), the presence of these diffuse scattering lines is related to the appearance of the 2D ordering.

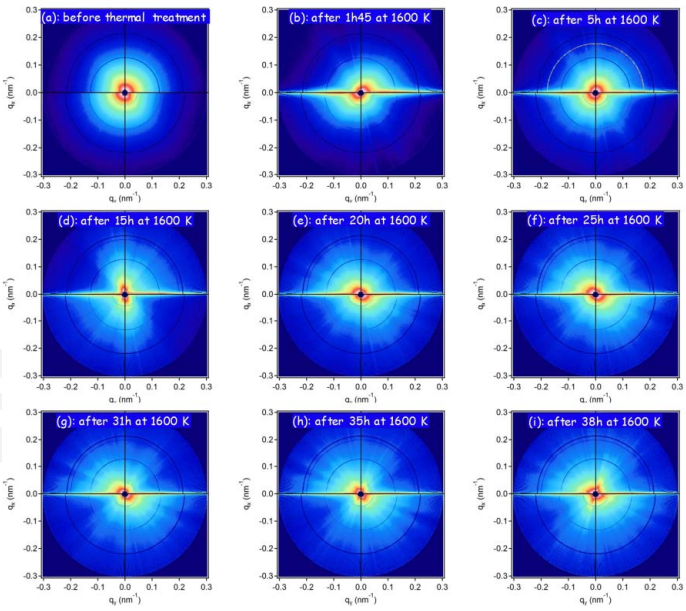

Figure 3. Self-organization of a sapphire vicinal surface during 40 hours of isothermal treatment at 1600 K and atmospheric pressure under pure oxygen flux.

We demonstrated with this experiment that, thanks to the QMAX furnace, 3D-GISAXS signals can be recorded *in situ* during a few tens of hours at very high temperatures under a controlled atmosphere.

4. Thermal expansion, phase transition and crystal growth in crystalline powders

In the previous example, the sample was a single crystal and the true temperature was determined thanks to the measurement of the position of one of the RLN of the sample itself. Of course such an approach is more difficult to implement for the characterization of powdered samples. We thus realized a (006) oriented single crystalline sample holder made of a cylindrical piece of sapphire in which we machined a 0.5 millimeter deep counterbore that can be filled by the sample powder. A small dot of sapphire is preserved in the center of this sample holder (see fig. 4a). At each set-point temperature, the true temperature can be determined through the measurement of the positions of the 0,0,6 and 0,0,12 RLNs of sapphire. A typical illustration of the discrepancy between the temperature target and the measured ones is reported in fig. 4b in the range between 400 to 2000 K. At low temperature, the sample temperature is higher than the set-point one, this gap is certainly related to the use of a Pt-10%Rh-Pt thermocouple that is not very efficient below 700 K. Between 700 and 1400 K the temperatures of the thermocouple and of the sample are close each other and a higher gap is observed for higher temperature. The maximal gap between the target and the measured value is roughly 60 K. This observation fully illustrates the interest of a direct measurement of the actual sample temperature that is the only one really interesting on the material characterization point of view.

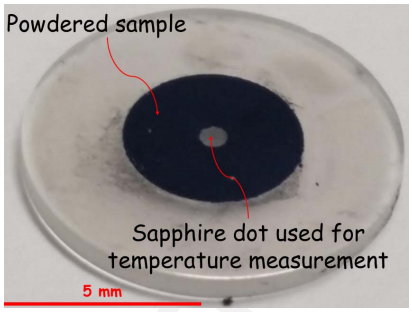

(a) The powders sample holder

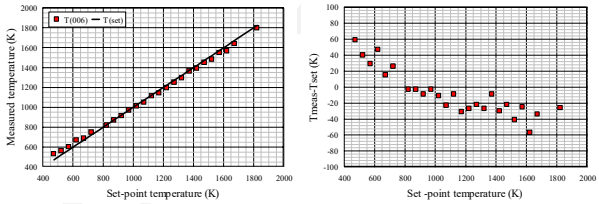

(b) evolution of the temperature determined with respect to the position of the sapphire 0,0,6 RLN as a function of the set-point temperature and evolution of discrepancy between the measured and set-point temperatures.

Figure 4. Sample holder for powders and measurement of the sample temperature.

Beside its ability to allow the determination of the sample temperature, the use of this single crystalline sample holder presents other interesting features. First of all, the procedure that we described to define with a very high accuracy the orientation of a single crystalline sample (§3) can be used for powdered samples. Such an accurate positioning of powdered samples can be of interest when rotation around the azimuthal axis is used or when the instrumental function needs to be optimized for high-resolution XRD measurements devoted to quantitative microstructural studies. The second important feature concerns the probed volume. For a number of reasons, XRD experiments realized at synchrotron radiation sources are often done using high-energy X-ray beams. The penetration depth is thus often of several hundreds of micrometers or higher. The use of a single crystalline sample holder allows the thickness of the probed volume to be strictly defined and thus the line broadening due to the sample transparency to be limited (Misture *et al.*, 1994).

Zirconium oxide, *i.e.* zirconia, is used for more than five decades in a very large number of applications spreading between high quality brick for glass furnaces, ceramic materials exhibiting high mechanical properties, thermal barrier coatings for aircrafts, solid-state ionic conductors for oxide full cells or basic compound of biomedical implants. In most cases, the production of zirconia materials requires the use of high or very high temperatures and in a large number of applications, these materials are used at high temperature. The knowledge of the thermal behavior of zirconia is thus essential. Under atmospheric pressure, pure zirconia (ZrO_2) exhibits two Solid-state Phase Transitions (SPTs) during cooling from the liquidus temperature. It solidifies into a cubic crystal structure ($Fm\bar{3}m$ space group) at about 3000 K, transforms to tetragonal ($P4_2/nmc$ space group) upon cooling to 2575 K and becomes monoclinic ($P2_1/c$ space group) at 1440 K (Smirnov *et al.*, 2003). Because of the values of the temperatures under consideration, it is a hard task to obtain accurate experimental data on the SPTs processes. As indicated above the tetragonal zirconia crystallized under the primitive $P4_2/nmc$ space group. Nevertheless, this structure is commonly described in the pseudo-cubic "face-centered tetragonal" lattice in which the crystallographic directions are parallel to those of the cubic form (see for example Kisi, 1998). This setting is very efficient in order to follow the m⇔t phase transition process. Accordingly, we adopt it all along this paper.

In 1994, R.J. Hill and M.D. Cranswick (Hill & Cranswick, 1994) published a paper reporting on a round robin test on the structure refinement through X-ray and neutron diffraction on powdered samples and the Rietveld method. This study was realized under the auspices of the International Union of Crystallography and two different samples were used. One of them was a powder of monoclinic zirconia synthesized by wet chemical route (referred below as "IUCr sample"), and we have recently used a small amount of it to show the capability of the QMAX furnace concerning XRD on powdered samples.

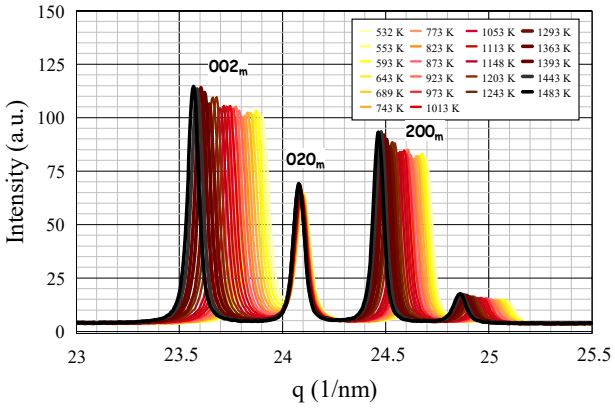

Figure 5. Anisotropy of the thermal expansion of monoclinic zirconia.

High temperature XRD patterns were recorded at 17.6 keV using a 2D pixel hybrid detector (XPAD) located at 800 mm from the sample onto the goniometer 2θ arm. We followed the structural evolutions of the powder between RT and 1800 K. At each temperature, 21 images were recorded in θ–2θ mode using a one-degree 2θ step between 8° and 28°. Only 5 s were needed for recording one image and the total signal was thus obtained in less than 2 minutes. The 21 2D-images were merged and integrated using a special class (multi-geometry) of the pyFAI library (Ashiotis *et al.*, 2015) to

reconstruct 1D diffraction patterns. The part of the reciprocal space explored was between 12 and 55 nm^{-1} that contains all the significant diffraction peaks of the different zirconia phases.

A part of the patterns recorded between RT and 1500 K is reported in fig. 5. This picture is a very clear observation of the strong anisotropy of the thermal expansion of monoclinic zirconia. Expansion along the $\vec{a}$ and $\vec{c}$ cell vectors is very significant. Simultaneously the β angle decreases (not shown here). On the contrary, the *b* cell parameter is quasi constant whatever the temperature is. The discussion on this observation is out of the scope of this article, nevertheless it can be noticed that such an anisotropy will generate in zirconia-based bulk materials large and anisotropic residual stresses.

Thermal treatments at higher temperature induce the monoclinic to tetragonal SPT and the reverse process during cooling down. XRD patterns were recorded every 10 K or even 5 K between 800 and 1800 K. Some of these patterns illustrating the SPTs are reported in fig. 6. The m →t transition starts at around 1450 K and at 1630 K all the crystals are under the tetragonal symmetry. The reverse transition, t→m starts close to 1450 K and ends below 1150 K. We show here that even in this powdered sample *a priori* free of any internal stresses, the phase transition process extends over more than 200 K. The t⇔m phase transition in zirconia is a first order one and it is of martensitic type. According to R.J. Hill (Hill, 1992) the mean size of the zirconia crystals in the pristine sample is equal to 62 nm. The temperature spreading of the phase transition and the thermal hysteresis are related to size and microstrain effects that we will not discuss here.

Since Scherrer's pioneering work in 1918 (Scherrer, 1918), it is well know that line profile analysis of the XRD peaks is an efficient way allowing the quantitative determination of the main microstructural parameters of powdered or bulk nanostructured polycrystalline materials. Very often, microstructural evolutions are

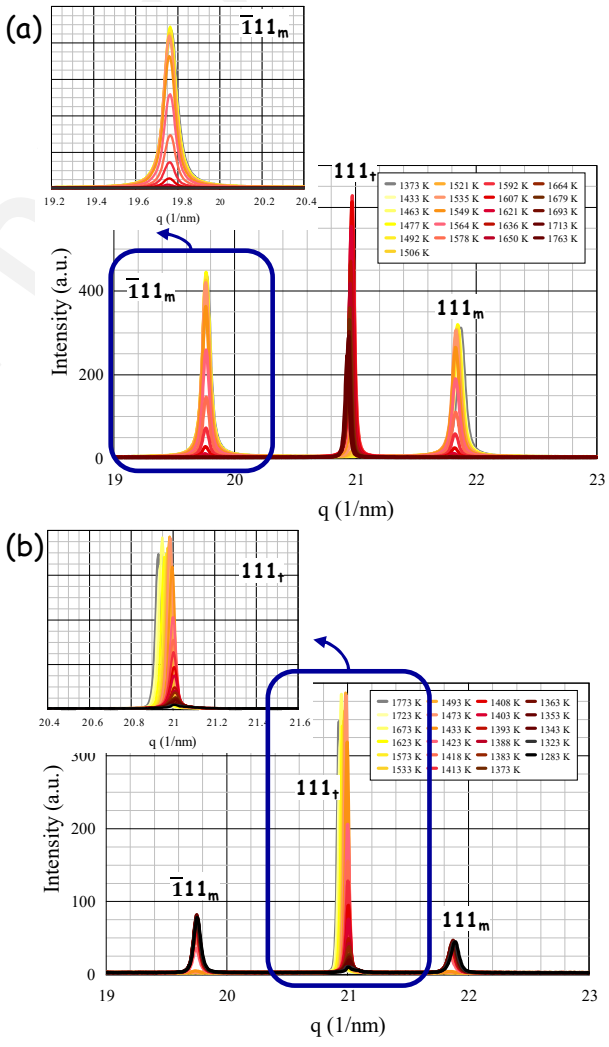

Figure 6. *in situ* observation between 1350 and 1800 K of the tetragonal ⇔monoclinic phase transition in the pure IUCr zirconia powder during respectively (a) the increase or (b) the decrease of the temperature.

not reversible and it is thus important to *in situ* catch processes such as crystal growth, microstrains relaxation, as well as variation of the density of stacking faults or dislocations. We studied the microstructural evolution of the IUCr zirconia sample during a 9 hours isothermal treatment at 1773 K under airflow. As written above, each full pattern is recorded in less than 2 minutes. Such measurements will allow to extract with high accuracy the kinetic of crystal growth and this will be presented in a forthcoming paper. The isothermal evolution at 1773 K of the 111 tetragonal zirconia peak is reported in fig. 7a where one pattern every half an hour is shown. The diffracted intensity is normalized and reported in log-scale. We observed all along the isothermal treatment a clear condensation of the diffuse scattering. The peak narrows in width and its profile evolves with a decrease of its Lorentzian part.

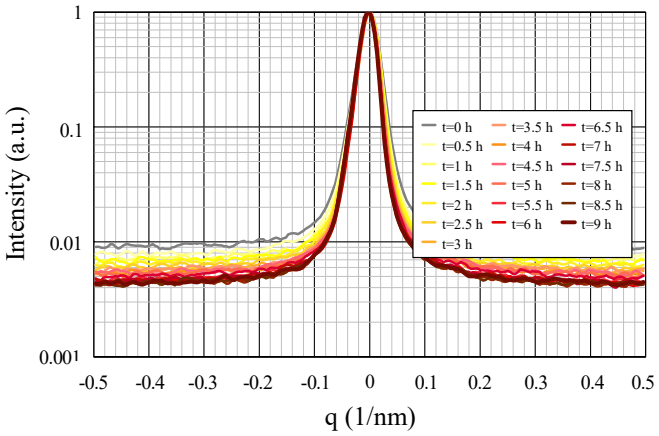

(a) evolution of the profile of the 111 tetragonal diffraction peak during the isothermal treatment.

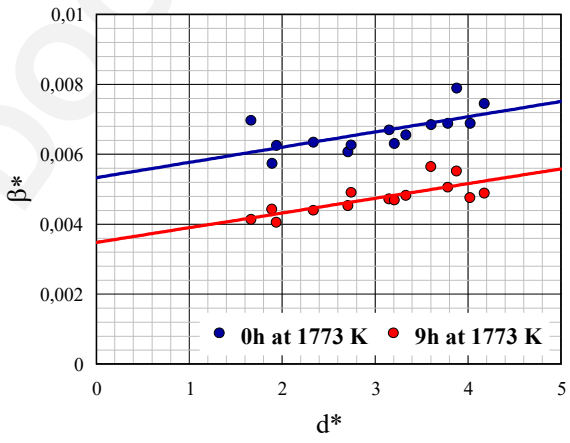

b) Williamson-Hall plot

Figure 7. *in situ* study of the tetragonal zirconia crystals growth in the IUCr pure zirconia powder during a 9 hours isotherm at 1773 K.

As a preliminary result, a Voigt function was used to fit the diffraction peaks of the first and the last patterns recorded during the isothermal treatment. Following the Williamson and Hall approach (Williamson & Hall, 1953), we plotted, the evolution of $\beta^* = \beta \cos\theta / \lambda$ (where β is the full width at half maximum of the diffraction peaks) as a function of the reciprocal space vector length d^* (see fig. 7b). According to the y-intercepts of the straight lines, the mean size of the tetragonal crystals evolves from 190 to 290 nm during the whole isotherm at 1773 K. Moreover, when looking at the slopes of the corresponding linear fits, it seems that the amount of microstrains stays roughly constant all along the isothermal treatment.

5. Phase transition and diffuse scattering into bulk polycrystalline samples

The physical properties of bulk metallic alloys as well as ceramics materials are often significantly different from those of the powders of the same compounds. In fact, residual stresses appearing during the synthesis of bulk materials through fuse cast or sintering processes have very often a strong

influence on the behavior of the materials under external constrains. The ability to determine the structural and microstructural evolutions *in situ* in bulk samples is thus often a key point for the development of new objects or devices. The QMAX furnace was built in such a way that it allows the characterization of bulk polycrystalline samples under conditions similar to those used for powdered samples. Samples exhibiting a typical surface of one square centimeter and a thickness of one millimeter can be put on top of the furnace, glued or not on a ceramic coating deposited on the heating element. As for the two first examples, the sample temperature was determined through the measurement of the thermal expansion α-alumina. Nevertheless, in that case we used a powder instead of a single crystal. Before the experiment, a thin layer of NIST SRM 676a alumina powder was spread onto the bulk samples surface and we determined the sample temperature according to the thermal evolution of both the *a* and *c* cell parameters of α-alumina.

As an illustration of high-temperature *in situ* XRD experiments on polycrystalline bulk samples, we studied ceramic dense samples that are part of large zirconia blocks elaborated through a specific fused cast process developed by the St Gobain company in order to manufacture large bricks (sub-meter scale) used as refractory components in industrial furnaces devoted to the production of glass. The sample was made of sub-millimeter zirconia dendrites embedded into a silica based glassy phase and it contains 95 % of pure zirconia. More details about the microstructure of this material have been published elsewhere (Patapy *et al.*, 2013). The XRD patterns were collected at 17.9 keV just below the zirconium absorption edge using the same 2D-pixel hybrid detector as for the experiments on powdered samples (see previous section). Taking into account of both the energy and the incidence angle of the X-ray beam, the penetration depth was close to one hundred of microns. Finally, according to the sub-millimeter size of this beam, the probed volume was in all cases smaller than one dendrite. We have shown previously (Örs

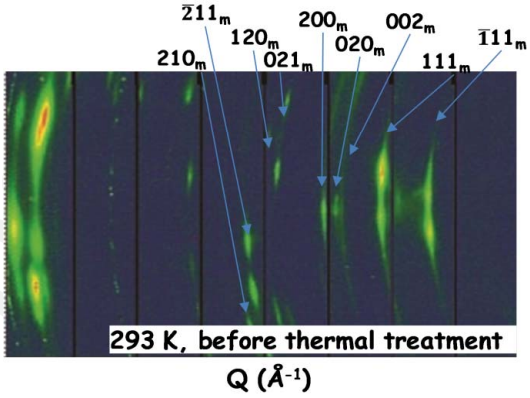

(a) Part of Debye-Scherrer rings diffracted by one zirconia dendrite.

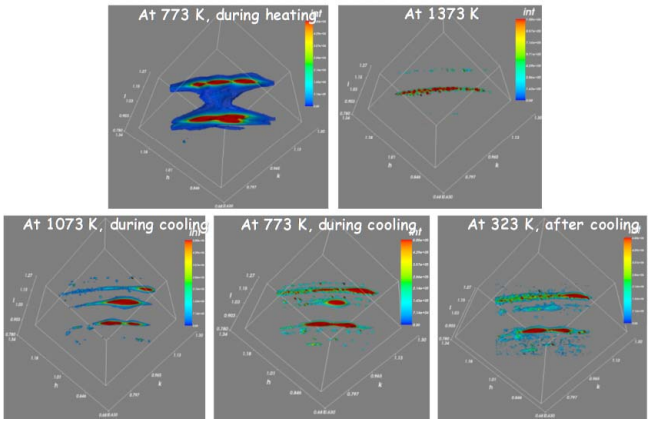

(b) 3D-reciprocal space maps around the around the $\bar{1}$,1,1 and 1,1,1 monoclinic RLNs at high temperature.

Figure 8. Phase transitions, diffuse scattering and stresses relaxation at high temperature in a bulk zirconia ceramic sample.

et al., 2018) through Laue microdiffraction that each dendrite can be considered to be mechanically independent to the rest of the sample. Moreover, we have demonstrated (Humbert *et al.*, 2010) that all monoclinic crystals constituting at RT one dendrite result in fact from the two successive SPTs (*i.e.* cubic →tetragonal and tetragonal →monoclinic) of one unique initial cubic crystal.

Part of the Debye-Scherrer rings recorded on such a sample at RT is reported in fig. 8a. This diffraction pattern shows that the diffracted intensity is located in specific areas along the Debye-Scherrer rings. This feature is due to crystallographic texture effect induced by the SPTs and it avoids to perform conventional extraction of a 1D diffraction pattern through radial integration of the Debye-Scherrer rings. On the contrary, it means that some crystals having a similar crystallographic orientation are diffracting in a specific part of the reciprocal space.

All the crystals diffracting at RT in this part of the reciprocal space correspond to crystals having the same orientation under the tetragonal form. Taking into account this global common orientation, we were able to find another RLN of the same set of monoclinic crystals and to fully determine in 3D the global orientation of these crystals. Finally, we have recorded 3D RSMs through *hkl*-scans close to the 1,1,1 tetragonal RLN as a function of the temperature up to 1473 K. At each considered temperature, two hundred 2D maps were recorded in roughly 1 hour. The 3D maps were reconstructed using a python routine developed at the D2AM beamline. The evolution of the diffuse scattering signal is illustrated in fig. 8b.

According to the loss of the 3-fold symmetry of the cubic space group around the [*hhh*] axis, each monoclinic node is in fact split into 3 different maxima. At 1373 K a large part of the zirconia crystals are under the tetragonal form and the diffuse scattering has roughly disappeared. Decrease of the temperature induces reappearance of a weaker diffuse scattering signal. This feature is clearly due to a coupling between strain relaxation and t⇔m phase transition. The volume of the monoclinic cell is roughly 4% higher than that of the tetragonal cell, and therefore during heating, the m→t transition is associated to stress relaxation. On the contrary, the reverse t→m transition induces the appearance of huge stresses that are partially relaxed by the formation of a microcrack network around the monoclinic crystals (Kisi, 1998). Description of this whole feature and of the interdependency of size and strain effects requires micromechanical modeling and is far from the topic of this paper. Nevertheless, we have shown here that using the QMAX furnace the coupled strain and diffuse scattering evolution on polycrystalline samples can be *in situ* captured at high temperature.

6. *In situ* oxidation of metal under controlled atmosphere

In all the experimental cases presented above, the measurements were done under air or oxygen flux and because the studied samples were oxides, no chemical reaction between the sample and the surrounding atmosphere was expected. As a last illustration of the capabilities of the QMAX furnace, we present an *in situ* reactive high-temperature time-resolved experiment. The samples were flat

plates of zirconium alloy and the general aim of the study was to understand the oxidation of this metallic alloy submitted to quick variations of the temperature up to 1450 K under oxygen rich atmosphere. According to the literature, in the range from 975 to 1450 K, the kinetics of the oxidization process of zirconium alloy strongly depends on the temperature. Very fast processes are expected at high temperature and our aim was to follow the formation of the oxide with a time resolution of about one minute during heating and one second during isothermal treatments. All the diffraction patterns were recorded using a large 2D-pixel hybrid detector (XPAD-WOS) available at the beamline and allowing a large part of the Debye-Scherrer rings to be recorded without any detector movement. This detector was fixed on the 2θ goniometer arm and the energy of the X-ray beam was fixed at 17.6 keV. The position of the detector was fixed at 850 mm from the specimen in such a way that, according to the energy of the X-ray beam, the oxide diffraction main peaks are clearly visible between the main diffraction peaks of zirconium alloy (see fig. 9a).

Because of the kinetics of the oxidation process, measurement of the sample temperature was a tricky part of the experiment. It was monitored via two thermocouples, one fixed on the heating resistor, and one spot-welded directly on the specimen surface. Accurate temperature was also determined by following the evolution of the cell parameters of the NIST SRM 676a alumina powder placed top of the sample.

The main stumble point with respect to the realization of reactive experiments able to capture structural evolutions of samples lies in the control of the gas atmosphere. Thanks to the use of the two gas lines linked to the furnace (see §2), we were able to monitor the composition of a

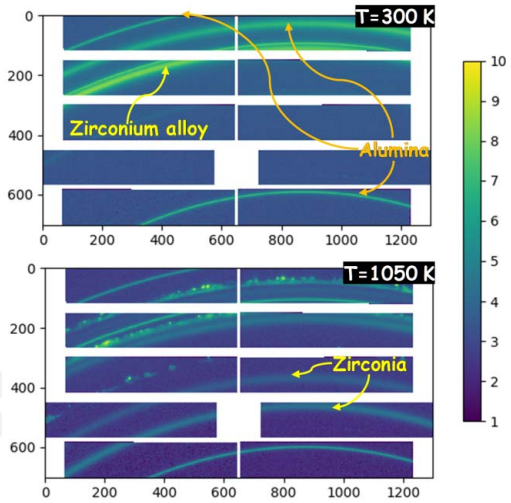

(a) Part of the Debye-Scherrer rings observed at RT and close to 1050 K. Two diffraction rings corresponding to the diffraction by zirconia crystals are clearly visible at high temperature.

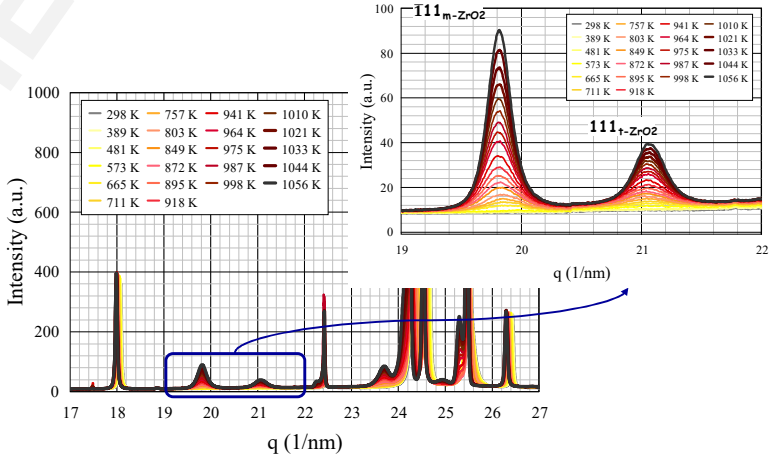

(b) Evolution of the XRD patterns during heating at 20 K/min between RT and 1100 K.

Figure 9. Oxidation of a zirconium based alloy at high temperature under controlled atmosphere of He-O_2 reactive gas mixture.

helium-oxygen gas mixture as a function of time and temperature through a computer-controlled process. As illustration, we report in fig. 9b the evolution of the diffraction patterns evidencing the oxidation of zirconium during heating from RT to 1050 K at a rate of 20 K/min and under a 1000 mL/min flux of 90%He-10%O_2 gas mixture. Patterns were recorded every 30 s. For sake of clarity, below 500 °C, only a few patterns are reported in fig. 9b. At higher temperatures, half of the recorded patterns are shown, which thus roughly corresponds to temperature steps of 20 K.

One of the aims of the study was to follow the relative amount of monoclinic and tetragonal zirconia appearing under oxidation atmosphere. The zirconia crystals have a size between a few nanometers and a few tens of nanometers, and the relative amount of tetragonal and monoclinic phases is strongly related to the size of these nanocrystals. We were able to follow the evolution of the mean size of both tetragonal and monoclinic zirconia crystals through line profile analysis during isothermal treatment realized at different temperatures between 700 °C and 1000 °C with a time scale of ten seconds.

7. Concluding remarks

We built-up through a 5-years collaborating research program funded by the ANR (ANR-09-NANO-031), a unique high temperature furnace implemented at the D2AM beamline at the ESRF. X-ray scattering or diffraction measurements can be done up to 2000 K under controlled gas flux at atmospheric pressure under reflection geometry. We have shown with the above description of four strongly different cases that this QMAX furnace is well-adapted for GISAXS or GID experiments as well as asymmetric or symmetric XRD on powdered or bulk samples under inert or reactive gas mixtures. The association of the QMAX furnace and up to date 2D pixel hybrid detectors allows the full exploration of the reciprocal space everywhere above the sample plane.

Thanks to the presence of a high precision motorized goniometric head on top of the D2AM kappa diffractometer, the translational and angular positions of the samples can be precisely adjusted as a function of temperature, and at any temperature, with an accuracy of a few tens of microns and few hundredth degree. We have also shown that we were able to keep this high precision positioning during two days at a temperature as high as 1600 K.

The development of devices based on nanostructured materials requires to be able to follow the evolution of their microstructure during their elaboration process or *operando*. Nowadays, it is clear that *in situ* or *operando* X-ray scattering set-ups have to be built using 2D, or a least 1D, position sensitive detector. Although lot of work is currently done to obtain high angular resolution using 2D position sensitive detectors (see for example Dejoie *et al.*, 2018), under reflection geometry the resolution remains directly linked to the beam size. We demonstrate that thanks to the high flux provided by the synchrotron radiation source and in spite of the use of a highly collimated parallel primary X-ray beam, high resolution XRD patterns can be recorded at the second time scale and full 3D RSM can be obtained in a few minutes. Such a time scale is very well suited for a large part of the

X-ray scattering measurements needed in the field of material science. These results open the field of experiments devoted to the *in situ* determination of the microstructure evolution of nanostructured materials at high temperature. We have shown that the study of nanocrystal growth can be performed at 1775 K on the zirconia IUCr standard sample and we observed relaxation of residual stresses into bulk ceramic materials through a high temperature phase transition.

External constrains can be the temperature, it can also be the evolution of the atmosphere surrounding the samples. The QMAX furnace has been designed to work under atmospheric pressure. It is thus easy to realize any type of X-ray scattering measurements at high temperature under controlled flux of gas mixture. The chemical reactions between single crystals as well as powdered or bulk polycrystalline samples with various types of gas mixture can thus be followed during isothermal treatments or during high speed heating or cooling.

Acknowledgements The QMAX furnace has been designed and built-up as a part of the QMAX Project No. ANR-09-NANO-031 funded by the French National Research Agency (ANR). We acknowledge the ESRF and the French Collaborating Research Group (F-CRG) for provision of synchrotron radiation facilities beamtimes. H. Song is thanked for his work on the preliminary thermomechanical calculations and the general sizing of the furnace. The build-up of the furnace has been realized under the technical supervision of D. de Barros. The experiments on the sapphire vicinal surfaces and on the IUCr zirconia powder were realized with the valuable help of C. Matringe (IRCER) and J.B. Marijon (PIMM) respectively. The authors are thankful to I. Cabodi and O. Bories (Saint-Gobain CREE) for the supply of the bulk zirconia based materials. Experiments on these bulk samples were done in the frame of the ASZTECH research program funded by the ANR (ANR-12-RMNP-0007). M. Huger and F. Gouraud from IRCER lab. and T. Örs and V. Michel from the PIMM lab. are strongly acknowledged for their implication during these experiments. The oxidation experiments were realized in the frame of a research program funded by the CEA Paris-Saclay centre in collaboration with R. Guillou, M. Lesaux, D. Menut and J.L. Bechade who are also strongly acknowledged.

References

Ago, H., Imamoto, K., Ishigami, N., Ohdo, R., Ikeda, K.I. & Tsuji, M. (2007). *Appl. Phys. Lett.* **90**, 133112.

Ashiotis G., Deschildre A., Nawaz Z., Wright J.P., Karkoulis D., Picca F.E., Kieffer J. (2015). *J. Appl. Cryst.* **48**, 510-519.

Bachelet, R., Cottrino, S., Nahélou, G., Coudert, V., Boulle, A., Soulestin, B., Rossignol, F., Guinebretière, R. & Dauger, A. (2007a). *Nanotechnology* **18**, 015301.

Bachelet, R., Boulle, A., Soulestin, B., Rossignol, F., Guinebretière, R. & Dauger A. (2007b). *Thin Solid Films* **515** ,7080-7085.

Basolo, S., Berar, J.F., Boudet, N., Breugnon, P., Caillot, B., Clemens, J.C., Delpierre, P., Dinkespiler, B., Hustache, S., Koudobine, I., Meessen, Ch., Menouni, M., Mouget, C., Palancher, H., Pangaud, P. Potheau, R. & Vigeolas E. (2007). *J. Synch. Rad.* **14**, 151-157.

Beck, M. & Mittemeijer, E.J. (2002). *J. Appl. Cryst.* **35**, 103-107.

Bénard, P., Auffrédic, J.P.& Louër, D. (1996). *Mater. Sci. Forum* **228-231**, 325-334.

Bergamaschi, A., Cervellino, A., Dinapoli, R., Gozzo, F., Henrich, B., Johnson, I., Kraft, P., Mozzanica, A., Schmitt, B. & Shi X. (2010). *J. Synch. Rad.* **17**, 653-668.

Boulle, A., Masson, O., Guinebretière, R. & Dauger, A. (2001). *Appl. Surf. Sci.* **180**, 322-327.

Boulle, A., Kilburger, S., Di Bin, P., Millon, E., Di Bin, C., Guinebretière, R. & Bessaudou, A. (2009). *J. Phys. D: Appl. Phys.* **42**,145403.

Brown, N. E., Swapp, S. M., Bennet, C. L. & Navrotsky, A. (1993). *J. Appl. Cryst.* **26**, 77-81.

Camelio, S., Babonneau, D., Lantiat, D. & Simonot, L. (2007). *EPL* **79**, 47002.

Chahine, G.A., Blanc, N., Arnaud, S., de Geuser, F., Guinebretière, R. & Boudet, N. (2019). *Metals* **9**, 352.

Cornelius, T.W., Davydok, A., Jacques, V.L.R., Grifone, R., Shülli, T., Richard, M.I., Beutier, G., Verdier, M., Metzger, T.H., Pietsch, U. & Thomas, O. (2012). *J. Synch. Rad.* **19**, 688-694.

Dejoie, C., Coduri, M., Petitdemange S., Giacobbe, C., Covacci, E., Grimaldi, O., Autran P.O., Mogodi, M.W., Jung, D.S. & Fitch, A.N. (2018). *J. Appl. Cryst.* **51**, 1721-1733.

Eaton, S.W., Fu, A., Wong, A.B., Ning, C.Z. & Yang, P.D. (2016). *Nat. Rev. Mater.* **1**, 16028.

Estermann, M., Reifler, H., Steurer, W., Fisler, F., Kocher, P. & Gauckler, L.J. (1999). *J. Appl. Cryst.* **32**, 833-836.

Gualtieri, A.F., Mazzucato, E., Venturelli, P., Viani, A. Zannini, P. & Petras, L. (1999). *J. Appl. Cryst.* **32**, 808-813.

Guinebretière, R. (2007). *X-ray diffraction on polycrystalline materials,* ISTE Ltd London.

Guinebretière, R., Boulle, A., Bachelet, R., Masson, O. & Thomas, P. (2007). *J. Appl. Cryst.* **40**, 332-337.

Hill, R.J. (1992). *J. Appl. Cryst*. **25**, 589-610.

Hill, R.J. & Cranswick J.M.D. (1994). *J. Appl. Cryst.* **27**, 802-844

Huang, M.H., Mao, S., Feick, H., Yan, H.Q., Wu, Y.Y., Kind, H., Weber, E., Russo, R. & Yang, P.D. (2001). *Science* **292**, 1897-1899.

Humbert, M., Gey, N., Patapy, C., Joussein, E., Huger, M., Guinebretière, R., Chotard, T. & Hazotte, A. (2010). *Scripta Mater.* **63**, 411-414.

Kisi, E. (1998). *Zirconia engineering ceramics. Old challenges - new ideas*, Trans Tech Publications, Zürich, Switzerland.

Koester, R., Hwang, J.S., Salomon, D., Chen, X., Bougerol, C., Barnes, J.P., Dang, D.L.S., Rigutti, L., Bugallo, A.L., Jacopin, G., Tchernycheva, M., Durand, C. & Eymery, J. (2011). *Nano Lett.* **11**, 43839-43845.

Koppelhuber-Bitschnau, B., Mautner, F.A., Worsch, P. & Gautsch, J. (1996). *Mater. Sci. Forum* **228-231**, 137-142.

Kotnik, P., Hofbauer, P., Resel, R., Koini, M., Haber, T. & Keckes, J. (2006). *Acta Cryst. A* **62**, s158.

Leake, S.J., Gilbert A. Chahine, G.A., Hamid Djazouli, H., Zhou, T., Richter, C., Hilhorst, J., Petit, L., Richard, M.I., Morawe, C., Barrett, R., Zhang, L., Homs-Regojo, R.A, Favre-Nicolin, V., Boesecke, P. & Schülli T.U. (2019). *J. Synch. Rad.* **26**, 571-584.

Lee, G.H. (2007). *Mater. Sci. Eng. B* **138**, 41-45.

Le Bourlot, C., Landois, P., Djaziri, S., Renault, P.-O., Le Bourhis, E., Goudeau, P., Pinault, M., Mayne-L-Hermite, M., Bacroix, B., Faurie, D., Castelnau, O., Launois, P. & Rouzière, S. (2012). *J. App. Cryst.*, **45**, 38-47.

Masson, O., Guinebretière, R. & Dauger, A. (1996). *J. Appl. Cryst.* **29**, 540-546.

Matringe, C., Fakih, A., Thune, E., Babonneau, D., Arnaud, S., Blanc, N, Boudet, N. & Guinebretière R. (2017). *Appl. Phys. Lett.* **111**, 031601.

Matringe, C., Thune, E., Cavalotti, R., Fakih, A., Arnaud, S., Blanc, N, Boudet, N., Coati, A., Garreau, Y., Babonneau, D. & Guinebretière R. (2020). S*ubmitted*.

Matringe, C. (2016) PhD thesis, University of Limoges, France.

Medjoubi, K., Bucaille, T., Hustache, S., Berar, J.-F., Boudet, N., Clemens, J.-C., Delpierre, P. & Dinkespiler, B. (2010). *J. Synchr. Rad.* **17**, 486–495.

Misbah, C., Pierre-Louis, O. & Saito Y. (2010). *Rev. Modern Phys.* **82**, 981-1040.

Misture, S. T., Hubbard, C. R. &Wang, X. L. (2002). *Adv. X-ray Anal.* **45**, 25-30.

Misture, S.T., Chatfield, L.R. & Snyder, R.L. (1994). *Powder Diffraction* **9**, 172-179.

Muller, F., Rannou, I., Duclaux, L. & Guer, J.M. (1997). *J. Appl. Cryst.* **30**, 557-558.

Montano, A. & Oyanagi H. (1999). Editors. *In situ synchrotron radiation research in materials science*, MRS Bull. **24**, n°1. Materials Research Society, Warrendale, USA.

Nakamura, S. (1998). *Science* **281**, 956-961.

Örs, T., Micha, J.S., Gey, N., Michel, V., Castelnau, O. & Guinebretière, R. (2018). *J. Appl. Cryst.* **51**, 55-67.

Örs, T., Ranc, N., Pelerin, M., Michel, V., Favier, V., Castelnau, O., Mocuta, C., and Thiaudière, D. (2019). *J. Synchr. Rad.* **26**, 1-11.

Patapy, C., Huger, M., Chotard, T., Guinebretiere, R., Gey, N., Hazotte, A. & Humbert, M. (2013). *J. Eur. Ceram. Soc.* **33**, 259–268

Pickup, D.M., Mountjoy, G. Roberts, M.A., Wallidge, G.W., Newport, R.J. & Smith, M.E. (2000). *J. Phys. Cond. Matter* **12**, 3521-3529.

Sarin, P., Haggerty, R.P., Yoon, W., Knapp, M., Berghaeuser, A., Zschack, P., Karapetrova, E., Yang, N. & Kriven, W.M. (2009). *J. Synch. Rad.* **16**, 273-282.

Scherrer P., (1918). *Nachrichten von der Gesellschaft der Wissenschaften zu Gottingen Mathematisch Physikalische*, **1-2**, 96-100.

Smirnov, M., Mirgorodsky, A. & Guinebretière R. (2003). *Phys. Rev. B* **68**, 104106.

Tao, F. & Salmeron, M. (2011). *Science* **331**, 171-174.

Thune, E., Fakih, A., Matringe, C., Babonneau, D. & Guinebretière R. (2017). *J. Appl. Phys.* **121**, 015301.

Touloukian, Y.S., Kirby, R.K., Taylor, R.E. & Lee, T.Y.R (1977). in *Thermophysical properties of matter*, ed. New York Plenum, **13**, 173-193.

Villanova, J., Daudin, R., Lhuissier, P., Jauffrès, D., Lou, S., Martin, C.L., Labouré, S., Tucoulou, R., Martinez-Criado, G. & Salvo, L. (2017). *Materials Today* **20**, 354359.

Williamson, G.K., & Hall W.H. (1953). *Acta Met.*, **1**, 22-31.

Yashima, M. (2002). *J. Am. Ceram. Soc.* **85**, 2925-2930.

Yashima, M., & Tanaka, M. (2004). *J. Appl. Cryst.* **37**, 786-790.

Yashima, M., Oh-Uchi, K., Tanaka, M. & Ida, T. (2006). *J. Am. Ceram. Soc.* **89**, 1395-1399.

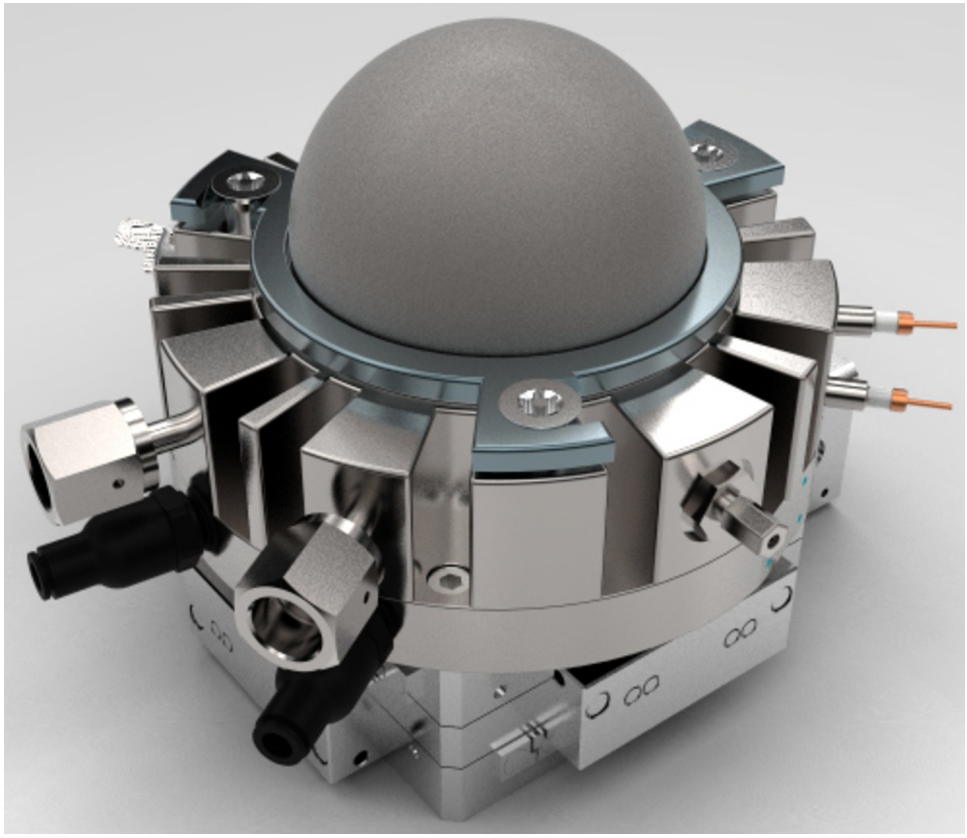

Figure 1a

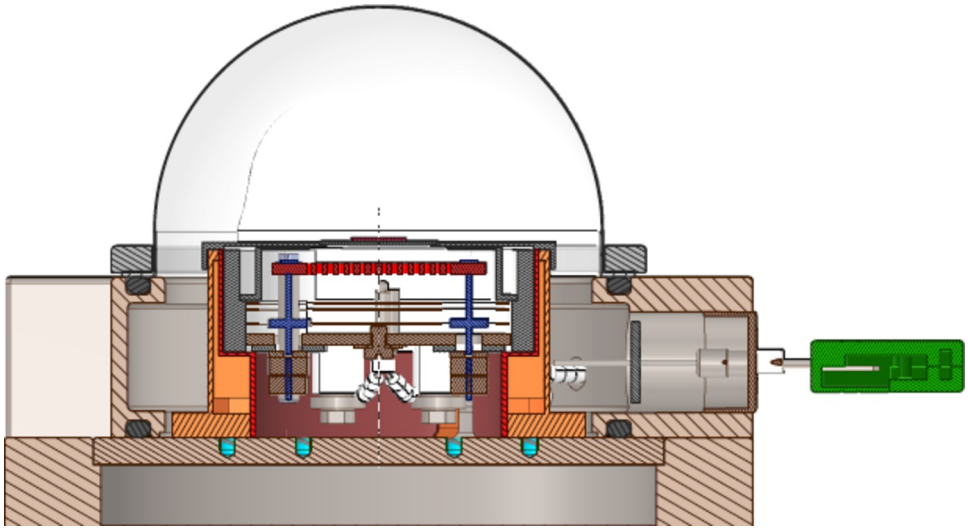

Figure 1b

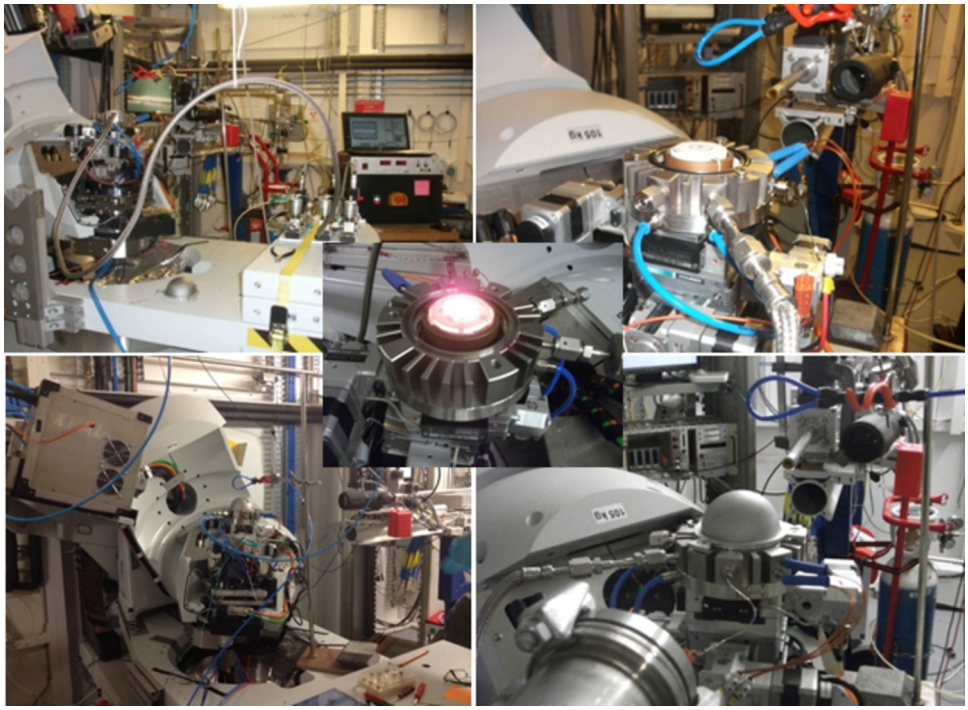

Figure 1c

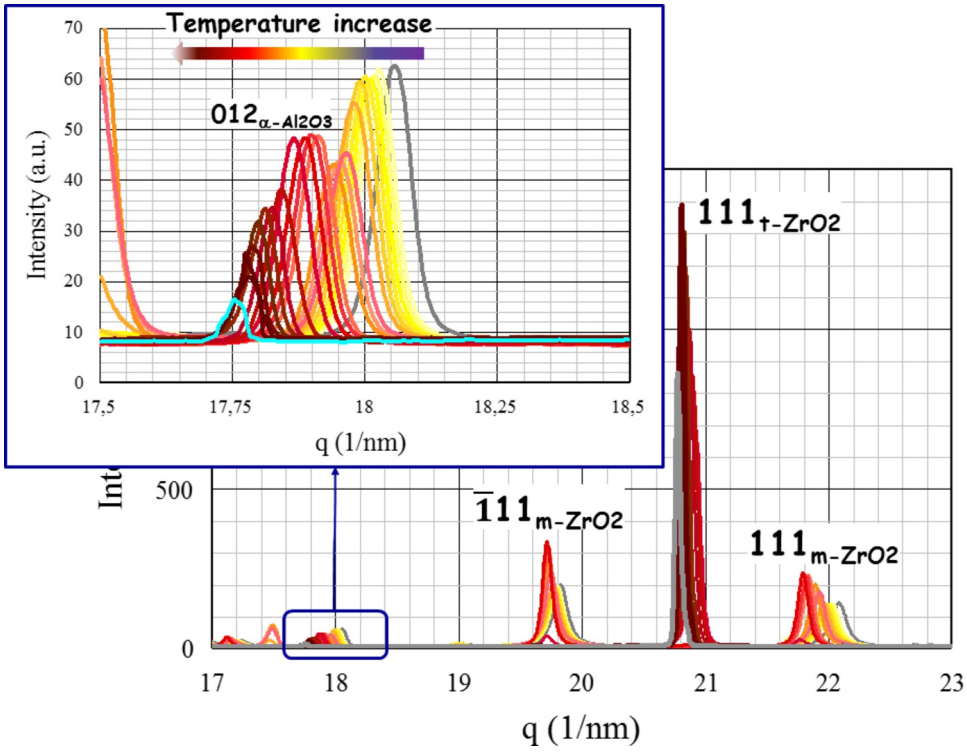
Temperature increase
012α-Al2O3
Intensity (a.u.)
70
60
50
40
30
20
10
0
17,5
17,75
18
18,25
18,5
q (1/nm)
111t-ZrO2
111m-ZrO2
111m-ZrO2
500
0
17
18
19
20
21
22
23
q (1/nm)

Figure 2

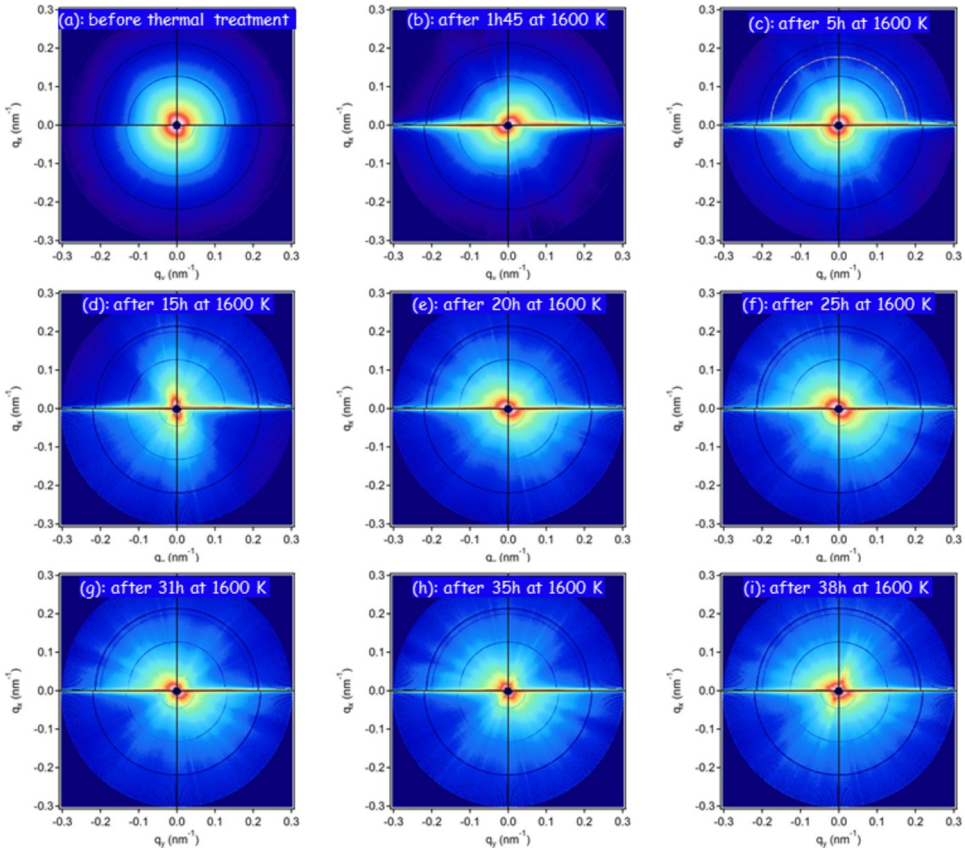
(a): before thermal treatment
(b): after 1h45 at 1600 K
(c): after 5h at 1600 K
(d): after 15h at 1600 K
(e): after 20h at 1600 K
(f): after 25h at 1600 K
(g): after 31h at 1600 K
(h): after 35h at 1600 K
(i): after 38h at 1600 K
q_z (nm^-1)
q_y (nm^-1)

Figure 3

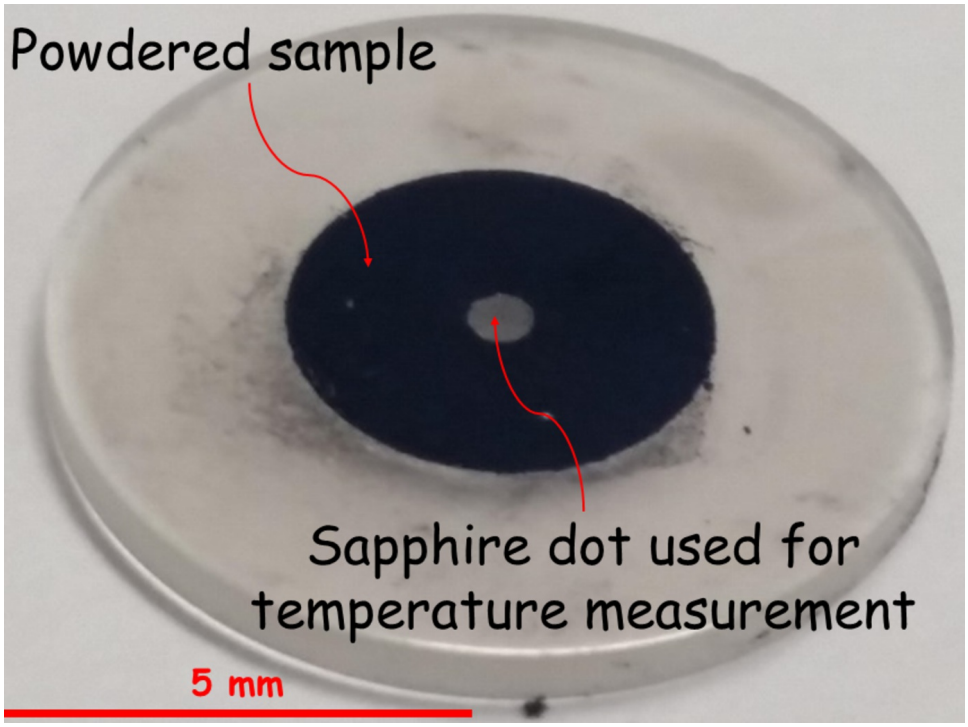
Powdered sample
Sapphire dot used for
temperature measurement
5 mm

Figure 4a

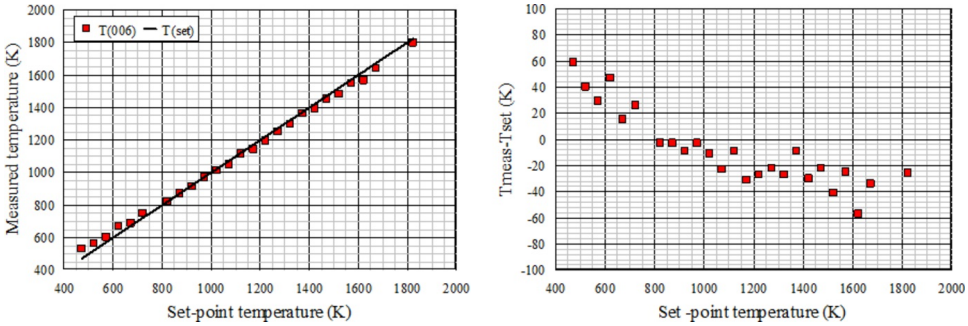
T(006)
T(set)
Measured temperature (K)
Set-point temperature (K)
Tmeas-Tset (K)
Set -point temperature (K)

Figure 4b

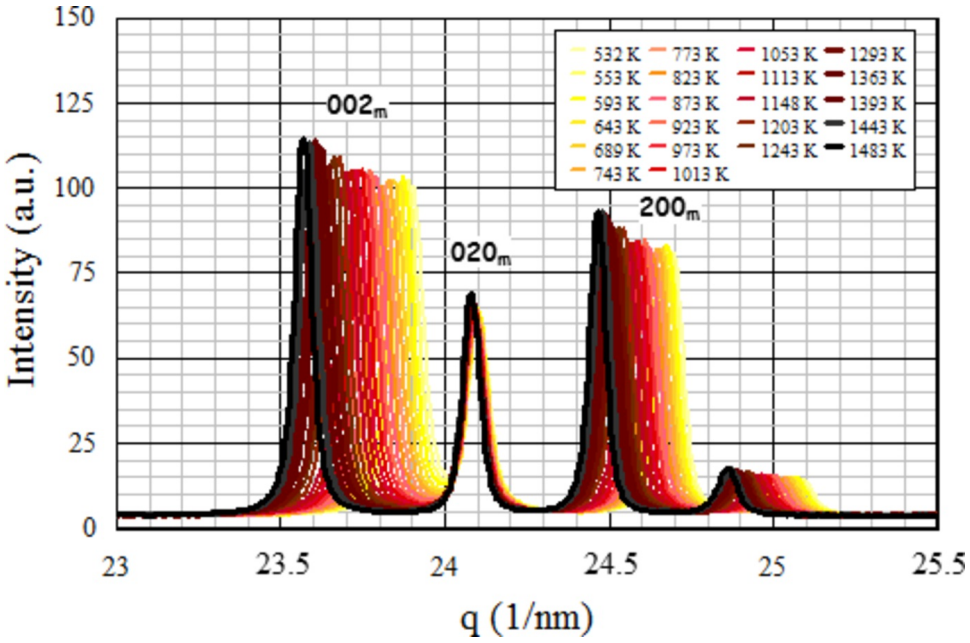
150
125
100
75
50
25
0
Intensity (a.u.)
23
23.5
24
24.5
25
25.5
q (1/nm)
002m
020m
200m
532 K
553 K
593 K
643 K
689 K
743 K
773 K
823 K
873 K
923 K
973 K
1013 K
1053 K
1113 K
1148 K
1203 K
1243 K
1293 K
1363 K
1393 K
1443 K
1483 K

Figure 5

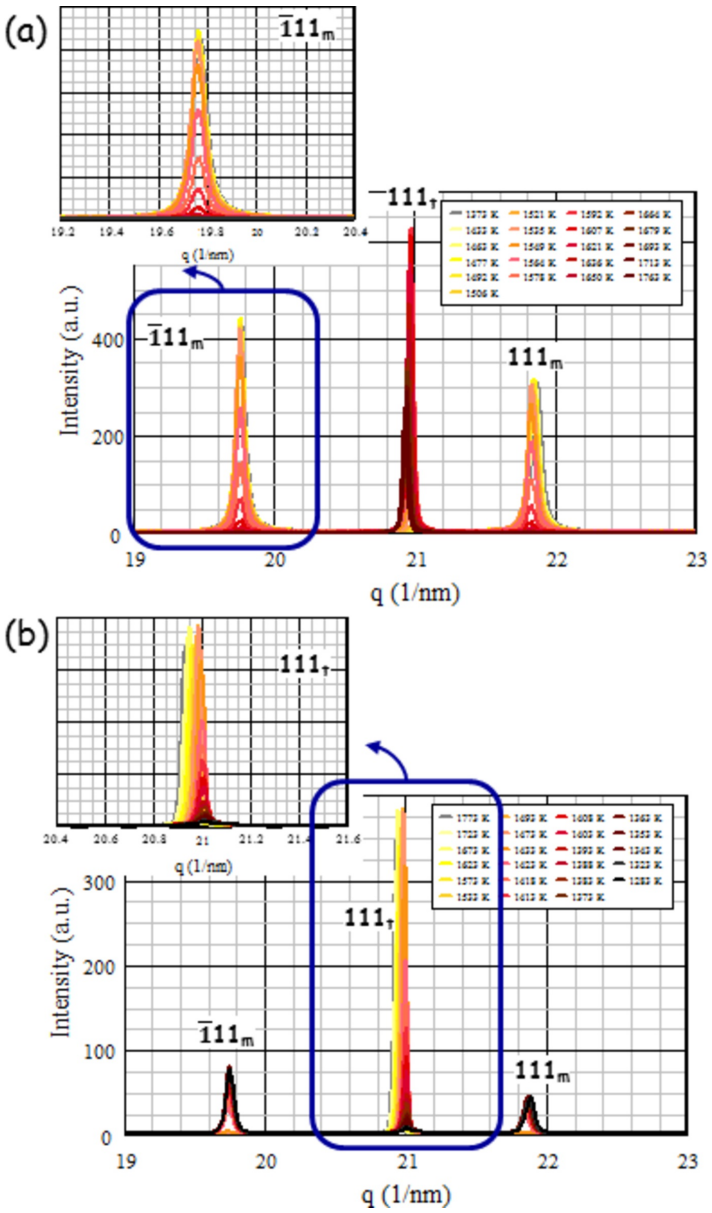
(a)
$\bar{1}11_m$
111_τ
111_m
Intensity (a.u.)
q (1/nm)
(b)
111_τ
$\bar{1}11_m$
111_m
Intensity (a.u.)
q (1/nm)

Figure 6

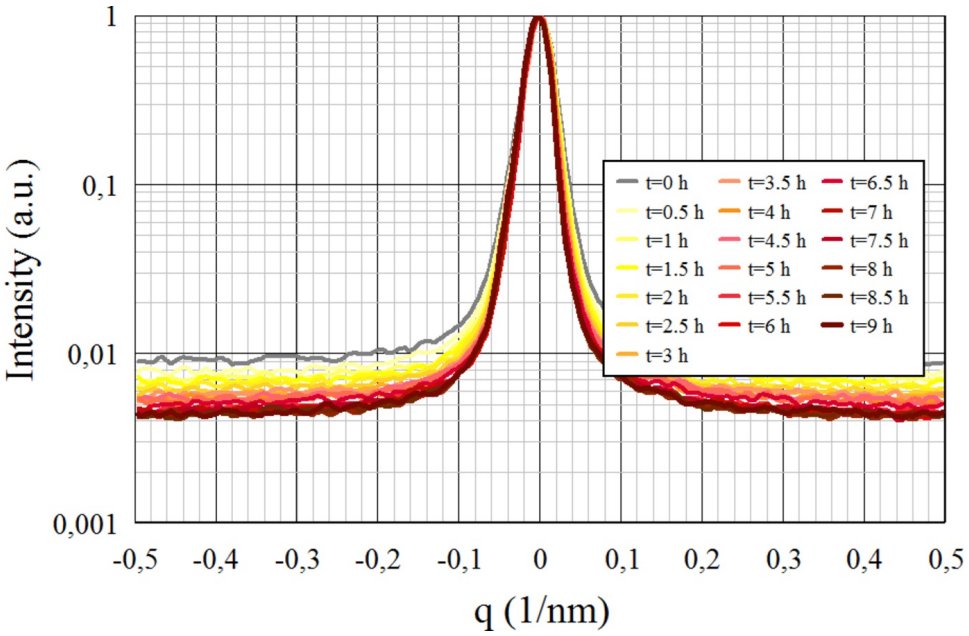
Intensity (a.u.)
1
0,1
0,01
0,001
-0,5
-0,4
-0,3
-0,2
-0,1
0
0,1
0,2
0,3
0,4
0,5
q (1/nm)
t=0 h
t=0.5 h
t=1 h
t=1.5 h
t=2 h
t=2.5 h
t=3 h
t=3.5 h
t=4 h
t=4.5 h
t=5 h
t=5.5 h
t=6 h
t=6.5 h
t=7 h
t=7.5 h
t=8 h
t=8.5 h
t=9 h

Figure 7a

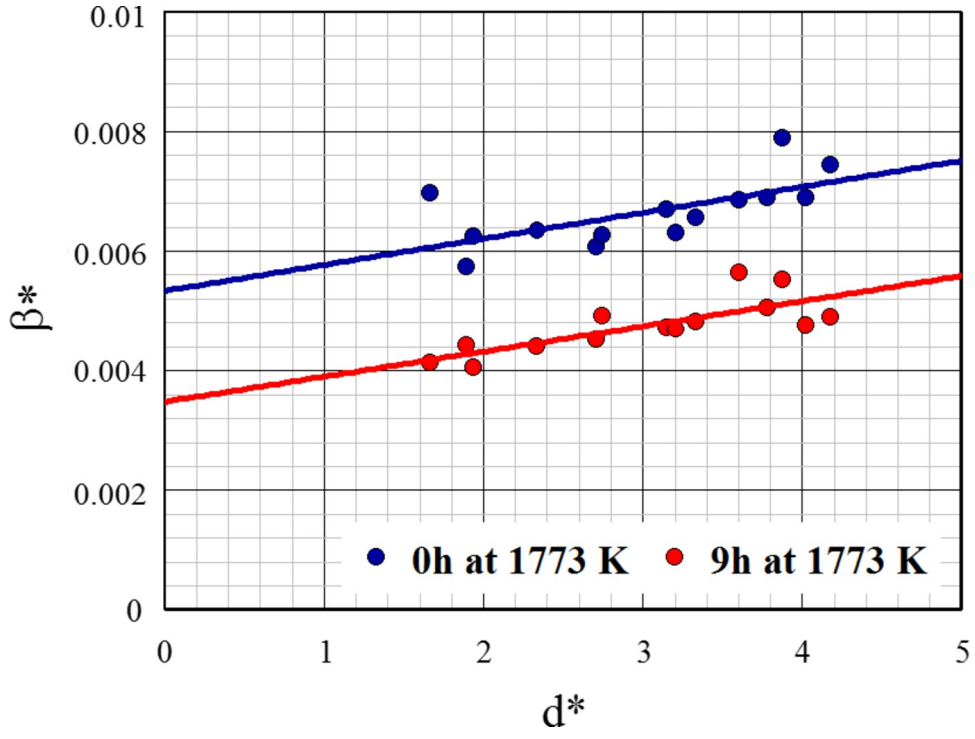

Figure 7b

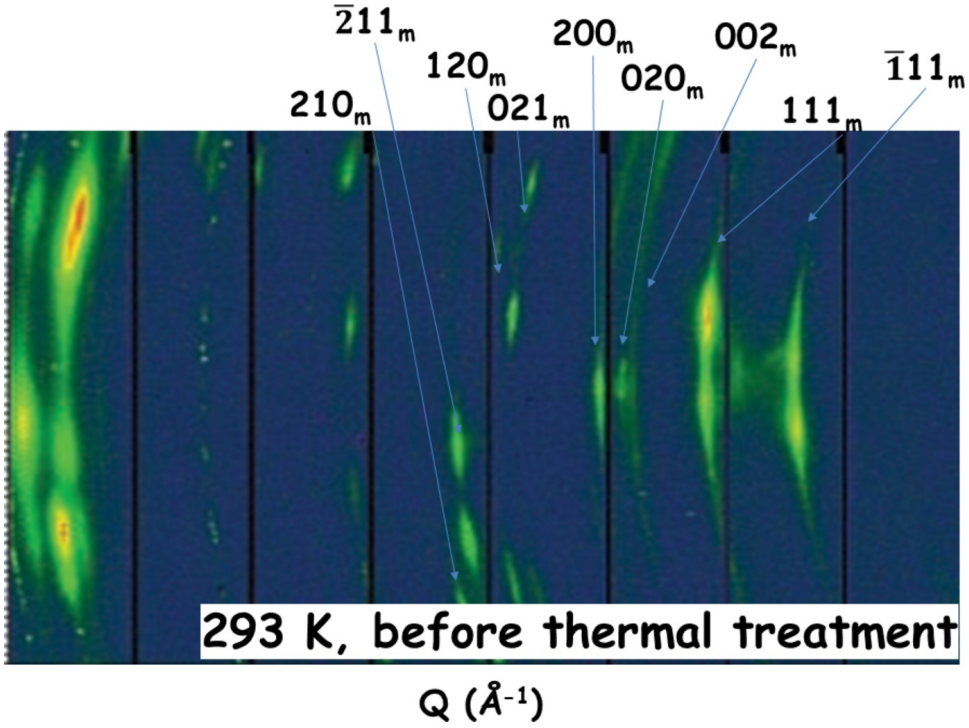
$\bar{2}11_m$
120_m
200_m
002_m
$\bar{1}11_m$
210_m
021_m
020_m
111_m
293 K, before thermal treatment
Q (Å^{-1})

Figure 8a

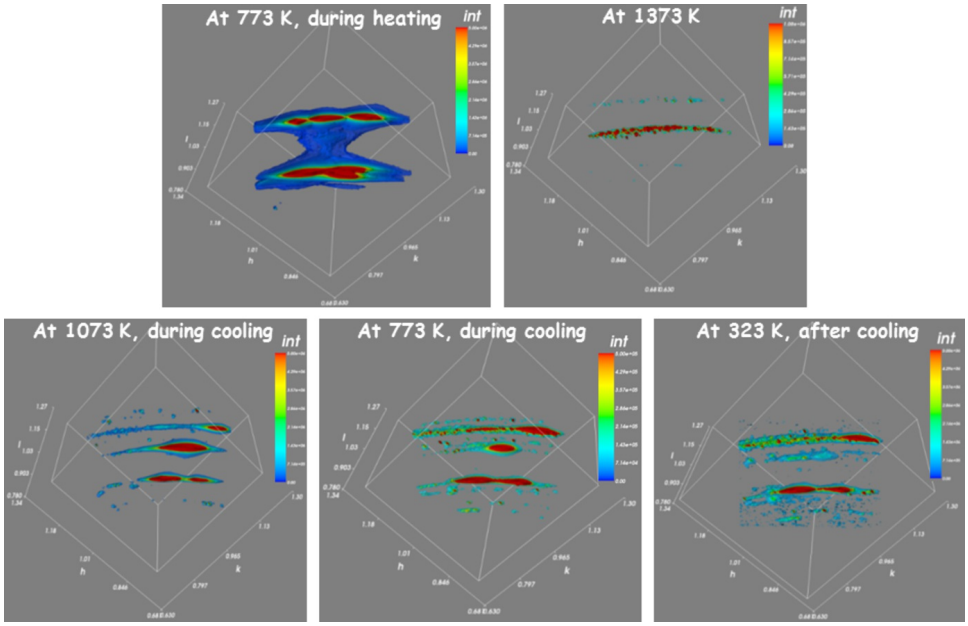
At 773 K, during heating
int
At 1373 K
int
At 1073 K, during cooling
int
At 773 K, during cooling
int
At 323 K, after cooling
int

Figure 8b

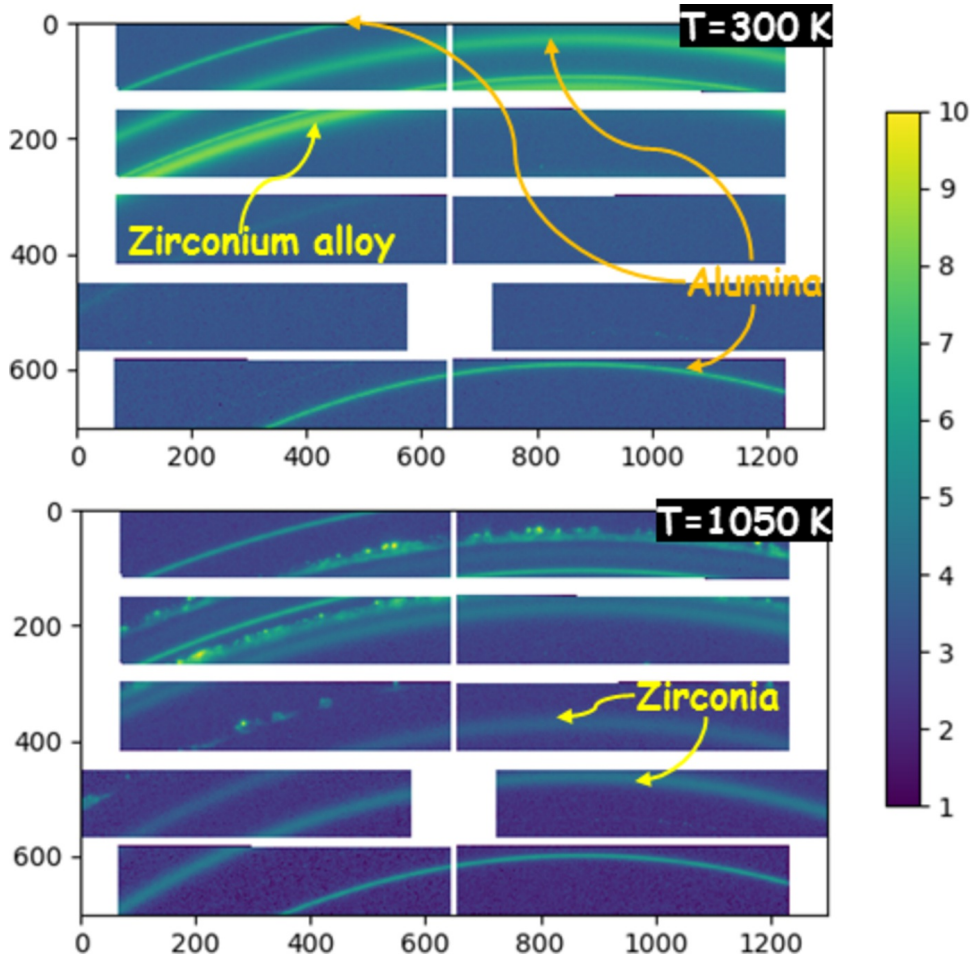
T = 300 K
Zirconium alloy
Alumina
T = 1050 K
Zirconia
0
200
400
600
800
1000
1200
1
2
3
4
5
6
7
8
9
10

Figure 9a

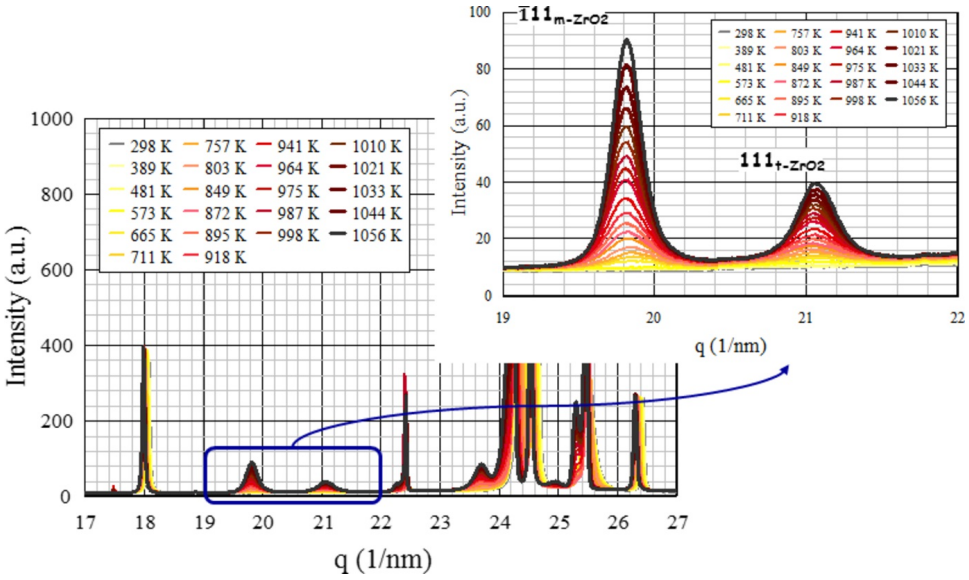
Intensity (a.u.)
q (1/nm)
298 K 757 K 941 K 1010 K
389 K 803 K 964 K 1021 K
481 K 849 K 975 K 1033 K
573 K 872 K 987 K 1044 K
665 K 895 K 998 K 1056 K
711 K 918 K
$\bar{1}11_{m\text{-}ZrO2}$
$111_{t\text{-}ZrO2}$

Figure 9b